

# Designing Weak Lensing Surveys: A Generalised Eigenmode Analysis

Martin Kilbinger<sup>1</sup> and Dipak Munshi<sup>2,3</sup>

<sup>1</sup>*Institut f. Astrophysik u. Extraterrestrische Forschung, Universität Bonn, Auf dem Hügel 71, D-53121 Bonn, Germany*

<sup>2</sup>*Institute of Astronomy, Madingley Road, Cambridge, CB3 0HA, United Kingdom*

<sup>3</sup>*Astrophysics Group, Cavendish Laboratory, Madingley Road, Cambridge CB3 0HE, United Kingdom*

7 November 2018

## ABSTRACT

We study the estimators of various second-order weak lensing statistics such as the shear correlation functions  $\xi_{\pm}$  and the aperture mass dispersion  $\langle M_{\text{ap}}^2 \rangle$  which can directly be constructed from weak lensing shear maps. We compare the efficiency with which these estimators can be used to constrain cosmological parameters. To this end we introduce the Karhunen-Loève (KL) eigenmode analysis techniques for weak lensing surveys. These tools are shown to be very effective as a diagnostics for optimising survey strategies. The usefulness of these tools to study the effect of angular binning, the depth and width of the survey and noise contributions due to intrinsic ellipticities and number density of source galaxies on the estimation of cosmological parameters is demonstrated. Results from independent analysis of various parameters and joint estimations are compared. We also study how degeneracies among various cosmological and survey parameters affect the eigenmodes associated with these parameters.

**Key words:** Cosmology: theory – gravitational lensing – large-scale structure of Universe – Methods: analytical, statistical, numerical

## 1 INTRODUCTION

Weak gravitational lensing studies (for a review see e.g. Mellier 1999; Bartelmann & Schneider 2001; Réfrégier 2003; van Waerbeke & Mellier 2003) probe the correlation of the observed ellipticities of background galaxies. Cosmic shear provides unbiased estimates of the matter power spectrum and hence can help us to place independent constraints on cosmological parameters (see e.g. Hu 1999). The parameter degeneracies from weak lensing surveys are very different from those present in CMB studies (van Waerbeke et al. 2002). This means that even most precise measurements from CMB observations can be improved by joint analyses with weak lensing data (Contaldi et al. 2003; Hu & Tegmark 1999). Thus, the recent detection of weak lensing by the large-scale structure (Bacon et al. 2000; Kaiser, Wilson & Luppino 2000; Wittman et al. 2000.; van Waerbeke et al. 2000, 2002; Maoli et al. 2001; Réfrégier, Rhodes & Growth 2002) has opened a completely new window to the Universe. While first generations of cosmic shear surveys have demonstrated the feasibility of weak lensing studies in constraining the dark matter power spectrum parametrised by  $\Omega_m$ ,  $\sigma_8$  and the shape parameter  $\Gamma$  (Réfrégier 2003; van Waerbeke, Mellier & Hoekstra 2005), future surveys will be able to probe much larger scales and therefore allow us to study the linear regime directly and put more stringent bounds on cosmolog-

ical parameters such as the equation of state of dark energy and its time variation.

As survey sizes grow the amount of data that is to be processed also increases. It is then essential to study data compression techniques which can effectively compress the data vector to a lower-dimensional space. The effect of such a compression on the Fisher information matrix can be studied by analysing the Karhunen-Loève (KL) eigenmodes (Karhunen 1947; Loève 1948) associated with the Fisher matrix. These techniques are already in use in cosmic microwave background studies (see e.g. Bond 1995 for COBE & FIRAS data, Bunn 1995 for COBE data and Tegmark, Taylor & Heavens 1997, hereafter TTH, for a general review of the KL eigenmode analysis). In the context of galaxy surveys, Matsubara, Szalay & Landy (2000) applied KL methods to the Las Campanas redshift survey, Hamilton, Tegmark & Padmanabhan (2000) studied PSCz using KL techniques and Szalay et al. (2003) have used this method to study data from SDSS. Watkins et al. (2001) have used these techniques to analyse the peculiar velocity surveys for removal of small-scale, non-linear modes from large-scale linear modes which retain cosmological information. Other studies using the KL eigenmode methods for velocity field surveys include Hoffmann & Zaroubi (2000) and Silberman et al. (2001). Recent studies by Huterer & White (2005)

have underlined its importance for filtering unwanted non-cosmological information at small angular scales.

The data vector in weak lensing surveys which is used to extract cosmological information is usually the shear correlation at various angular separations, estimated from the shapes of the observed background galaxies. Thus, it represents an already compressed data set for which likelihood analyses are feasible although further compression can speed up the analysis. Moreover, for third-order statistics, the number of measured triangle configurations can be very large even in a binned way and further compression of the data might be necessary to place constraints in a high-dimensional cosmological parameter space. Therefore, the study of KL methods in the context of cosmic shear will be very useful for future weak lensing surveys.

Being not only an effective tool for data compression, the KL eigenmode analysis can also help to understand the specific linear combination of angular scales and the redshift range that contributes most significantly to a specific estimator. A KL eigenmode analysis of weak lensing observables in redshift space has already been done in by Heavens (2003), where the distribution of observed ellipticities was directly used as data vector. We extend these analyses to second-order shear statistics as functions of projected angular scales and for realistic survey geometries. The latter issue is particularly interesting as sky coverage in any weak lensing survey will always be non-trivial due to the presence of bright foreground stars and galaxies. Our study therefore gives us useful clues about the survey design. We provide a KL eigenmode analysis for the second-order shear measures  $\xi_{\pm}$ ,  $\xi_{\text{tot}}$  and  $\langle M_{\text{ap}}^2 \rangle$  (to be defined later). The covariance of these estimators were studied in detail by Schneider et al. (2002) to assess the effect of source ellipticity dispersion and finite sky coverage on the estimation of cosmological parameters. The influence of survey geometry was investigated in Kilbinger & Schneider (2004). We use those results to construct the Fisher matrix to forecast parameter constraints. In contrast to those previous studies, where the above mentioned second-order shear statistics were used to determine cosmological parameters, we also consider the parameter dependence of the covariance of these estimators and its influence on the Fisher matrix. Moreover, the KL approach allows us to study in detail how the convergence power spectrum is sampled on different scales by a given shear survey.

The paper is arranged in the following way. Section §2 is devoted to a recapitulation of the basics of the KL eigenmode analysis, reformatted in the weak lensing context. In section §3, we describe our simulations and survey strategies in detail (§3.1 – §3.3) and present the results for the eigenmode analysis (§3.4), including the effect of survey strategy, noise and binning. We discuss our findings in §4.

## 2 NOTATIONS AND FORMALISM

### 2.1 Survey characteristics

We consider several different survey strategies in this work. First, individual images are distributed randomly (but non-overlapping) within circular patches on the sky, where ‘image’ means one individual field of view of size  $13' \times 13'$ . The

individual patches are uncorrelated, thus the largest scale where the shear correlation can be measured is twice the patch radius. The random image placement accounts for the fact that for realistic surveys, bright stars and foreground galaxies should be avoided and therefore sparse sampling of a sky region is necessary.

A survey consists of  $P$  patches of radius  $R$ , each patch containing  $N$  images. The total number of images is 300 for all patch geometries, corresponding to 14.1 square degrees for the entire survey.

We use  $N = 30$  and  $R = 100', 140'$ , respectively. Note that the number of patches in a survey is  $P = 300/N$ . We denote these patch geometries by the two numbers  $(N, R)$ , thus we have the configurations  $(30, 100')$  and  $(30, 140')$ .

Second, we define two surveys which consist of single, uncorrelated fields of view with the same total area of 14.1 square degrees. The first survey consists of 75 uncorrelated  $26' \times 26'$  square images – typical fields of view for current wide-field cameras like WFI on the ESO 2.2-m telescope. The second survey represents 12 independent  $65' \times 65'$ -fields, corresponding to new-generation wide-field cameras like MegaCam/CFHT. We denote these surveys with  $75 \cdot 26'^2$  and  $12 \cdot 65'^2$ , respectively. A sketch of the geometry of the surveys used in this work can be found in Fig. 1.

If not indicated otherwise, the number density of source galaxies is  $n_{\text{gal}} = 30 \text{ arcmin}^{-2}$ . This number density of high-redshift galaxies which are usable for weak lensing shape measurements can be achieved with high-quality ground-based imaging data from a 4 m-class telescope. The source galaxy ellipticity dispersion is  $\sigma_{\varepsilon} = 0.3$ , if not stated otherwise.

### 2.2 Second-order shear statistics

The light of distant galaxies is deflected while propagating through the tidal gravitational potential of intervening matter inhomogeneities which constitute the large-scale structure in the Universe. The image of a galaxy gets distorted, and in the weak lensing approximation, the relation  $\varepsilon = \varepsilon^s + \gamma$  holds between the observed ellipticity  $\varepsilon$  of a galaxy, its intrinsic ellipticity  $\varepsilon^s$  and the shear  $\gamma = \gamma_1 + i\gamma_2$ . From the shear, one can in principle reconstruct the projected matter density or convergence  $\kappa$ .

For two points separated by a vector  $\boldsymbol{\theta}$  with polar angle  $\varphi$ , one defines the tangential and cross-component of the shear as

$$\gamma_t \equiv -\Re(\gamma e^{-2i\varphi}) \quad \text{and} \quad \gamma_{\times} \equiv -\Im(\gamma e^{-2i\varphi}). \quad (1)$$

The two shear two-point correlation functions (2PCF) and their relation to the convergence power spectrum  $P_{\kappa}$  are (Kaiser 1992)

$$\xi_{\pm}(\boldsymbol{\theta}) = \langle \gamma_t \gamma_t \rangle \pm \langle \gamma_{\times} \gamma_{\times} \rangle = \frac{1}{2\pi} \int_0^{\infty} d\ell \ell P_{\kappa}(\ell) J_{0,4}(\ell\theta), \quad (2)$$

where the first-kind Bessel function  $J_0$  ( $J_4$ ) corresponds to the ‘+’ (‘-’) correlation function.

A very useful second-order statistics is the dispersion of the so-called aperture mass (Kaiser 1995, Schneider 1996), which is the weighted tangential shear integrated over a circular aperture. When using a polynomial compensated filter

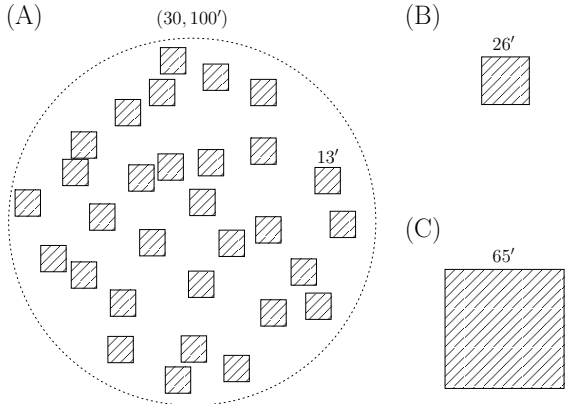


**Figure 1.** Sketch of the two kinds of survey strategies used in this work. On the left, a patch of  $100'$  radius is filled sparsely with 30 images of size  $13'$ , a survey consists of 10 such patches. For comparison, on the right the field sizes of surveys consisting of 75 uncorrelated  $26' \times 26'$  images and 12 independent  $65' \times 65'$  fields, respectively, are shown.

function as weight (Schneider 1996, Schneider et al. 1998), the dispersion of the aperture mass is related to the power spectrum by

$$\langle M_{\text{ap}}^2(\theta) \rangle = \frac{1}{2\pi} \int_0^\infty d\ell \ell P_\kappa(\ell) \left( \frac{24 J_4(\ell\theta)}{(\ell\theta)^2} \right)^2. \quad (3)$$

The aperture mass statistics is a measure of the E-mode only of cosmic shear. A similar statistics  $\langle M_\perp^2 \rangle$  can be defined as the weighted cross-component of shear in an aperture, which is a measure of the B-mode only. The aperture mass statistics yields the separate measurement of the E- and B-mode which allows one to quantify contaminations to the gravitational shear signal. A B-mode mainly comes from systematic measurement errors like imperfect PSF correction and/or intrinsic alignment of source galaxies, whose shape correlations are to be measured.

The 2PCF are easily obtained from real data however complicated the survey geometry might be. The two aperture statistics can be expressed in terms of the 2PCF:

$$\langle M_{\text{ap},\pm}^2(\theta) \rangle = \int_0^{2\theta} \frac{d\vartheta}{2\theta^2} \left[ \xi_+(\vartheta) T_+ \left( \frac{\vartheta}{\theta} \right) \pm \xi_-(\vartheta) T_- \left( \frac{\vartheta}{\theta} \right) \right], \quad (4)$$

where  $T_+$  and  $T_-$  are given explicitly in Schneider, van Waerbeke & Mellier (2002). In the absence of a B-mode, both terms on the right-hand side of the previous equation are of the same amplitude, resulting in  $\langle M_\perp^2 \rangle = 0$ .

An unbiased estimator of the shear 2PCF (2) for a set of (logarithmic) angular bins is given by

$$\hat{\xi}_\pm(\vartheta) = \frac{1}{N_p(\vartheta)} \sum_{ij} (\varepsilon_{it} \varepsilon_{jt} \pm \varepsilon_{i\times} \varepsilon_{j\times}), \quad (5)$$

where the sum goes over all pairs of galaxies, whose angular separation is in the angular bin corresponding to  $\vartheta$ .  $\varepsilon_i$  is the (complex) ellipticity of a galaxy at position  $\theta_i$  and  $N_p(\vartheta)$  is the number of pairs in the  $\vartheta$ -bin. Galaxies measured from real data might carry weight factors reflecting the individual noise and precision in the shape measurement. Using these weights, one can define a more optimal estimator for the

2PCF; however, we do not include this effect and assume equal weights for each galaxy.

Unbiased estimators for the dispersions of the two aperture mass statistics  $\langle M_{\text{ap}}^2 \rangle$  and  $\langle M_\perp^2 \rangle$  (4), respectively, are

$$\mathcal{M}_\pm(\theta) = \sum_{i=1}^I \frac{\Delta\vartheta_i \vartheta_i}{2\theta^2} \left[ \hat{\xi}_+(\vartheta_i) T_+ \left( \frac{\vartheta_i}{\theta} \right) \pm \hat{\xi}_-(\vartheta_i) T_- \left( \frac{\vartheta_i}{\theta} \right) \right], \quad (6)$$

where the limit  $I$  of the sum must be chosen such that  $\theta$  is half the upper limit of the  $I$ -th bin. For simplicity of notation, we will from now on identify the estimators with their corresponding shear statistics, and write  $\xi_+, \xi_-$  and  $\langle M_{\text{ap}}^2 \rangle$  for the estimators.

These second-order shear estimators are used extensively in the literature, including independent studies involving  $\xi_\pm$  or the joint data vector  $\xi_{\text{tot}} = (\xi_+, \xi_-)$ . We do not take into account the shear dispersion in an aperture  $\langle |\gamma|^2 \rangle$ . Although this estimator has a high signal-to-noise ratio and has been used extensively in the literature, it does not separate the E- from the B-mode, unlike the aperture mass statistics.

Schneider et al. (2002) calculated the covariance matrices  $\mathbf{C}$  of the estimators defined in this section, in the case of a Gaussian shear field. The covariances of the 2PCF consist of three terms: A pure shot noise term ( $\mathbf{D}$ ), originating from the dispersion of the intrinsic ellipticities of the source galaxies, present only on the diagonal, a cosmic variance term ( $\mathbf{V}$ ), and a mixed term ( $\mathbf{M}$ ):

$$\begin{aligned} \mathbf{C}_{++} &\equiv \mathbf{C}(\hat{\xi}_+, \vartheta_1; \hat{\xi}_+, \vartheta_2) = \mathbf{D} + \mathbf{M}_{++} + \mathbf{V}_{++} \\ \mathbf{C}_{--} &\equiv \mathbf{C}(\hat{\xi}_-, \vartheta_1; \hat{\xi}_-, \vartheta_2) = \mathbf{D} + \mathbf{M}_{--} + \mathbf{V}_{--} \\ \mathbf{C}_{+-} &\equiv \mathbf{C}(\hat{\xi}_+, \vartheta_1; \hat{\xi}_-, \vartheta_2) = \mathbf{M}_{+-} + \mathbf{V}_{+-}. \end{aligned} \quad (7)$$

The individual terms in full length are given in Schneider et al. (2002). The covariance of both of the aperture mass statistics,  $\mathbf{C}(\mathcal{M}_\pm)$ , can be calculated from the 2PCF covariance matrices using eq. (6).

Derivatives of the covariances with respect to cosmological parameter are easily obtained by differentiating eqs. (7). The shot-noise term, being independent of cosmology, does not contribute, and the cosmic variance term, being quadratic in the correlation function, has a larger influence than the mixed term.

The covariances of these estimators were studied in detail by Schneider et al. (2002), where covariance matrices were constructed using an ensemble average over galaxy positions. Kilbinger & Schneider (2004) calculated the covariances directly by summing over a specific realisation of galaxy positions which we follow here. This has the advantage of being able to handle the discreteness resulting from the finite galaxy number density in a correct way. Moreover, incorporations of realistic survey strategies is done in a natural way.

We note here that the cosmic variance term  $\mathbf{V}$  only contains the Gaussian or unconnected part of the four-point correlator of shear. On scales below  $\sim 10$  arc minutes, the non-Gaussianity of the shear field gets important (van Waerbeke et al. 2002; Scoccimarro, Zaldarriaga & Hui 1999). On scales below  $\sim 1$  arc minute the shot noise term  $\mathbf{D}$  dominates over  $\mathbf{V}$  (Kilbinger & Schneider 2004), thus under the

Gaussian assumption we expect to slightly underestimate the covariances in this transition regime between 1 and 10 arc minutes.

### 2.3 Fisher information matrix

The Fisher matrix (Kendall & Stuart 1969; TTH) is defined as

$$F_{\alpha\beta} = \left\langle \frac{\partial^2[-\ln \mathcal{L}]}{\partial p_\alpha \partial p_\beta} \right\rangle_{\mathbf{p}=\mathbf{p}_0} = \left( \frac{\partial^2[-\ln \mathcal{L}]}{\partial p_\alpha \partial p_\beta} \right)_{\mathbf{p}=\mathbf{p}_0}, \quad (8)$$

where the likelihood  $\mathcal{L}$  depends on a vector of model parameters  $\mathbf{p} = (p_1, p_2, \dots)$  and  $\mathbf{p}_0$  denotes the true parameter values. The Fisher matrix is the expectation value of the Hessian matrix of  $(-\ln \mathcal{L})$  at  $\mathbf{p} = \mathbf{p}_0$  and is roughly spoken a measure of how fast  $\mathcal{L}$  falls off from its maximum. The smallest possible variance  $\Delta p_\alpha$  of any unbiased estimator of some parameter  $p_\alpha$  is given by the Cramér-Rao inequality

$$\Delta p_\alpha \geq \sqrt{(F^{-1})_{\alpha\alpha}}; \quad (9)$$

the right-hand side of this inequality is called the minimum variance bound (MVB). If only one parameter is to be determined from the data and all others are fixed, the MVB simplifies to  $(F_{\alpha\alpha})^{-1/2}$ .

In the case of a Gaussian probability distribution function for the parameters, the Fisher matrix becomes (Bunn 1995; Vogley & Szalay 1996; TTH)

$$F_{\alpha\beta} = \frac{1}{2} \text{tr} [\mathbf{C}^{-1} \mathbf{C}_{,\alpha} \mathbf{C}^{-1} \mathbf{C}_{,\beta} + \mathbf{C}^{-1} \mathbf{M}_{\alpha\beta}]. \quad (10)$$

$\mathbf{C}_{,\alpha} \equiv \partial \mathbf{C} / \partial p_\alpha$  denotes the derivative of the covariance with respect to the  $\alpha^{\text{th}}$  parameter.  $\mathbf{M}_{\alpha\beta} = \boldsymbol{\mu}_{,\alpha} \boldsymbol{\mu}_{,\beta}^t + \boldsymbol{\mu}_{,\beta} \boldsymbol{\mu}_{,\alpha}^t$  where  $\boldsymbol{\mu}$  is mean of the data vector  $\mathbf{x}$ ,  $\langle \mathbf{x} \rangle = \boldsymbol{\mu}$ . In our case, the  $n$ -dimensional data vector  $\mathbf{x}$  consist of one or a combination of the second-order statistics of shear as defined in Sect. 2.2 (see also Sect. 3.1 for more details).

The  $m = 7$  parameters  $p_\alpha$  (cosmological parameters plus source galaxy redshift distribution characteristics) which we consider here are given in Sect. 3.2.

### 2.4 Karhunen-Loève (KL) eigenmodes and eigenvalues

A general linear data compression can be written as

$$\tilde{\mathbf{x}} = \mathbf{T} \mathbf{x}, \quad (11)$$

where from the  $n$ -dimensional data vector  $\mathbf{x}$  a new  $\tilde{n}$ -dimensional data set  $\tilde{\mathbf{x}}$  is constructed via the  $\tilde{n} \times n$  matrix  $\mathbf{T}$ . This means that the expectation value  $\langle \mathbf{x} \rangle$  of the original data vector  $\mathbf{x}$  transforms to  $\langle \tilde{\mathbf{x}} \rangle = \mathbf{T} \langle \mathbf{x} \rangle$  and hence the covariance  $\mathbf{C} = \langle \mathbf{x} \mathbf{x}^t \rangle - \langle \mathbf{x} \rangle \langle \mathbf{x} \rangle^t$  changes accordingly to  $\tilde{\mathbf{C}} = \mathbf{T} \mathbf{C} \mathbf{T}^t$ . In our case,  $\mathbf{x}$  consists of the shear correlation functions  $\xi_+$  and  $\xi_-$  or the aperture mass dispersion  $\langle M_{\text{ap}}^2 \rangle$ , representing  $n$  data points measured for various angular scales, see Sect. 3.1. An example for a data compression is already given in eq. (6):  $\langle M_{\text{ap}}^2 \rangle$  is a linearly compressed version of  $\xi_+$  and  $\xi_-$ , the compression matrix  $\mathbf{T}$  depends in this case on the functions  $T_+$  and  $T_-$ .

The Fisher matrix  $\mathbf{F}$  corresponding to the original data vector  $\mathbf{x}$  changes to  $\tilde{\mathbf{F}}$ , given by

$$\tilde{F}_{\alpha\beta} = \frac{1}{2} \text{tr} [(\mathbf{T} \mathbf{C} \mathbf{T}^t)^{-1} (\mathbf{T} \mathbf{C}_{,\alpha} \mathbf{T}^t) (\mathbf{T} \mathbf{C} \mathbf{T}^t)^{-1} (\mathbf{T} \mathbf{C}_{,\beta} \mathbf{T}^t)]$$

$$+(\mathbf{T} \mathbf{C} \mathbf{T}^t)^{-1} (\mathbf{T} \mathbf{M}_{\alpha\beta} \mathbf{T}^t)] \quad (12)$$

Clearly, when the dimensionality  $n$  and  $\tilde{n}$  of the original and the transformed data vectors are the same, the transformation is a similarity transformation and the Fisher matrix remains unchanged,  $\tilde{\mathbf{F}} = \mathbf{F}$ .

The goal of the KL analysis is to find a compression matrix  $\mathbf{T}$  for  $\tilde{n} < n$  without losing too much of information and to estimate cosmological parameters with as small error bars as possible. Considering the minimum variance bound (9) of some cosmological parameter  $p_\alpha$ , we seek to maximise the Fisher matrix element  $\tilde{F}_{\alpha\alpha}$ .

Following TTH, we first consider the two simple cases of a constant mean  $\boldsymbol{\mu}$  and a constant covariance  $\mathbf{C}$ , where constant means with respect to the parameter vector  $\mathbf{p}$ . Then, we optimise for several parameters simultaneously with the aid of a singular value decomposition (SVD).

For cosmic shear, the assumption of a constant covariance seems quite natural, since in most cases of weak lensing observations, the covariance is not calculated analytically but extracted directly from the data (e.g. van Waerbeke et al. 2002) and thus it is constant and not depending on cosmological parameters. However, the situation is different for the mean, since with a model parameter independent mean, it is not possible to even define a likelihood function. And although within the Fisher matrix formalism, a constant mean can be considered in a consistent way, this mean first has to be found using e.g. the maximum likelihood estimator. But the distinction into a constant mean and a constant covariance case is of rather technical nature, and the general case of parameter dependent mean and covariance can be considered by combining the two, see Sect. 2.4.3. Thus, a strategy to obtain cosmological parameters and their minimum variance bound from data would be first to define a likelihood function  $\mathcal{L}$  using a parameter dependent mean (and parameter dependent covariance if desired) to find the maximum likelihood parameter  $\mathbf{p}_0$ . Second, the Fisher matrix is calculated by evaluating the second derivatives of  $\mathcal{L}$  at the point  $\mathbf{p} = \mathbf{p}_0$ . A KL analysis and data compression can be undertaken by first considering the two cases of constant mean and covariance independently, and later combining both cases.

Note that in our case, the ‘‘mean’’ is a second-order statistics (the shear correlation), and the covariance is of fourth order (although reduced to only depend on second-order because of the assumption of a Gaussian shear field). We therefore choose a different approach than e.g. Heavens (2003) or Seljak (1998) who directly use the galaxy ellipticities as data vector. In their case, the (zero) mean is of first order, and the covariance contains the information about the power spectrum.

#### 2.4.1 Constant Mean

In the case where the mean  $\boldsymbol{\mu}$  is known and constant, the second term in (12) vanishes, since  $\boldsymbol{\mu}_{,\alpha} = 0$  and therefore  $\mathbf{M}_{\alpha\beta}$  vanishes, too. We first consider a compression matrix which consists of only one row vector,  $\mathbf{T} = \mathbf{b}^t$ . The task of maximising the Fisher matrix diagonal element  $F_{\alpha\alpha}$  in order to minimise the error bar on the cosmological parameter  $p_\alpha$  is then equivalent to maximising the eigenvalue  $\lambda$  of the generalised eigenproblem  $\mathbf{C}_{,\alpha} \mathbf{b} = \lambda \mathbf{C} \mathbf{b}$ . By Cholesky-decomposing the symmetric and positive definite covariance

matrix  $\mathbf{C} = \mathbf{L}\mathbf{L}^t$ , it can be reduced to the ordinary eigenproblem

$$(\mathbf{L}^t \mathbf{C}_{,\alpha} \mathbf{L}^{-t}) \mathbf{L}^t \mathbf{b} = \lambda \mathbf{L}^t \mathbf{b}. \quad (13)$$

Solving this equation for all  $n$  orthogonal eigenvectors  $\mathbf{L}^t \mathbf{b}_k$  gives us  $n$  real eigenvalues  $\lambda_k$ . A compression matrix  $\mathbf{T}$  is then constructed containing as row vectors the first  $\tilde{n}$  eigenvectors which have been sorted by the absolute value of their corresponding eigenvalues. The matrix  $\mathbf{T}$  represents a set of eigenvectors, rank-ordered according to their signal-to-noise ratio.

The KL eigenmodes defined in this way satisfy an orthogonality relation. Eigenmodes with high eigenvalues or low rank numbers contain more information about a specific parameter, whereas the ones with small (absolute) eigenvalues and high rank numbers contain almost no additional information. As will be shown in Sect. 3.3, we typically achieve a compression by a factor of nearly two for the independent analysis of various parameters with getting the same MVB as for the uncompressed case.

An individual eigenmode  $\mathbf{b}_k$  contributes to the measurement error for the parameter  $p_\alpha$  as  $\delta p_\alpha = 1/|\lambda_k|$ . Thus, the signal-to-noise ratio for this mode therefore is  $p_\alpha (\delta p_\alpha)^{-1} = p_\alpha |\lambda_k|$ .

The new Fisher matrix diagonal element  $\tilde{F}_{\alpha\alpha}$  corresponding to a KL compression with  $\tilde{n}$  eigenmodes is simply (TTH)

$$\tilde{F}_{\alpha\alpha} = \frac{1}{2} \sum_{k=1}^{\tilde{n}} \lambda_k^2. \quad (14)$$

In our analysis (Sect. 3.3), we repeat the data compression, starting from the second-order statistics  $\xi_\pm$  and  $\langle M_{\text{ap}}^2 \rangle$  given for  $n$  angular separations and plot for various cosmological parameters  $p_\alpha$  the associated error  $\Delta p_\alpha = 1/(\tilde{F}_{\alpha\alpha})^{1/2}$  as a function of  $\tilde{n}$ , where  $\tilde{n} \leq n$  is the dimension of the compressed data vector  $\tilde{\mathbf{x}}$ , see Fig. 2. Although being a decreasing function of  $\tilde{n}$ , the error reaches a constant plateau for some  $\tilde{n}_0 < n$ , thus the original error for the uncompressed case is recovered before all KL modes are used for the parameter estimation. We find in most of the cases that a plateau is reached for  $\tilde{n}_0 \lesssim n/2$ , thus a compression factor of nearly two is possible without any loss of information. This compression is with respect to the number of angular separations  $n$  at which the second-order shear statistics are measured, representing a binned version of the data vector comprising of all observed galaxy pairs. Note that the compression factor depends of course on the original number of bins — we comment on the binning in Sect. 3.3.6.

Since in the case of a constant mean, the Fisher matrix contains products of the inverse covariance and the (derivative of the) covariance, it is independent of the survey area, and very little sensitive of the survey geometry.

#### 2.4.2 Constant covariance

In contrast to the constant mean case, there is only one eigenvector which contains all of the available information when the covariance is known and independent of the parameters. In this case, the first term in (12) vanishes, and the corresponding eigenproblem is

$$(\mathbf{L}^{-1} \mathbf{M}_{\alpha\alpha} \mathbf{L}^{-t}) \mathbf{L}^t \mathbf{b} = \lambda \mathbf{L}^t \mathbf{b} \quad (15)$$

which has only one non-trivial solution  $\mathbf{L}^t \mathbf{b}_0 = \mathbf{L}^{-1} \boldsymbol{\mu}_{,\alpha}$  with eigenvalue  $\lambda_0 = 2|\mathbf{L}^{-1} \boldsymbol{\mu}_{,\alpha}| = \text{tr} [\mathbf{C}^{-1} \mathbf{M}_{\alpha\alpha}]$ .

Inserting the only eigenvector  $\mathbf{b}_0 = \mathbf{C}^{-1} \boldsymbol{\mu}_{,\alpha}$  for the compression matrix  $\mathbf{T}$  into (12), we find that the modified Fisher matrix is the same as the original one,  $\tilde{F}_{\alpha\beta} = F_{\alpha\beta} = \boldsymbol{\mu}_{,\alpha}^t \mathbf{C}^{-1} \boldsymbol{\mu}_{,\beta}$ . This is not surprising since all data is collected into one mode, and no information is lost.

If geometrical effects of the survey are neglected, the covariance is proportional to one over the survey area  $A$ . Thus, in the case of constant covariance the Fisher matrix is proportional to  $A$ , in contrast to the constant mean case, where  $\mathbf{F}$  is independent of  $A$ . For reasonable large cosmic shear surveys, the second term in (10) is therefore dominant over the first one (Sect. 3.3.5).

#### 2.4.3 General case

TTH describe how the general case (when neither mean nor covariance is constant) can be treated efficiently, by simply adding the one eigenmode from the constant covariance case to the  $\tilde{n}$  modes from the constant mean analysis. However, as mentioned in the previous section, the constant covariance eigenmode is (for reasonably large survey areas) dominant over all the other modes and contains the bulk part of the information about cosmological parameters. Thus, we do not consider to combine these two cases.

#### 2.4.4 Joint parameter estimation

For the independent estimation of a parameter  $p_\alpha$ , the KL method is devised to minimise the associated error bar  $\Delta p_\alpha = (\tilde{F}_{\alpha\alpha})^{-1/2}$  in a suitably rotated basis. However, for the case of joint parameter estimation, the object to be minimised is the diagonal of  $(\mathbf{F}^{-1})^{1/2}$  which is a more demanding optimisation problem. We follow TTH who discuss an alternative approximate technique which virtually does the same. The individual compression matrices  $\mathbf{T}_\alpha$ , optimised for the independent estimation of the parameter  $p_\alpha$ , are arranged into a new matrix after multiplying each row (which corresponds to an eigenvector) with its corresponding eigenvalue as  $\mathbf{T} = (\boldsymbol{\Lambda}_1 \mathbf{T}_1^t, \dots, \boldsymbol{\Lambda}_m \mathbf{T}_m^t)$ . Here,  $\boldsymbol{\Lambda}_\alpha = \text{diag}(\lambda_{\alpha 1}, \dots, \lambda_{\alpha n})$  is a diagonal matrix containing the eigenvalues corresponding to the individual eigenanalysis of the  $\alpha^{\text{th}}$  parameter.  $\mathbf{T}$  will contain a lot of redundant information, because of unavoidable near-degeneracies between parameters, e.g. between  $\Omega_m$  and  $\sigma_8$  or between  $\Gamma$  and  $n_s$ .

In order to separate useful from redundant information, this new matrix  $\mathbf{T}$  is factorised using a singular value decomposition (SVD),

$$\mathbf{T} = \left( \overbrace{\left( \boldsymbol{\Lambda}_1 \mathbf{T}_1^t \mid \dots \mid \boldsymbol{\Lambda}_m \mathbf{T}_m^t \right)}^{nm} \right) = \left( \overbrace{\mathbf{U}}^n \right) \cdot \left( \overbrace{\boldsymbol{\Sigma}}^n \right) \cdot \left( \overbrace{\mathbf{V}^t}^{nm} \right) \Bigg|_n,$$

where  $\mathbf{U}^t \mathbf{U} = \mathbf{V}^t \mathbf{V} = \mathbf{1}$  and  $\boldsymbol{\Sigma} = \text{diag}(\sigma_i)$  is a diagonal matrix containing the singular values  $\sigma_i$ , which can be interpreted as generalised eigenvalues. After sorting the columns of  $\mathbf{U}^t$  according to the absolute values of the corresponding  $\sigma_i$  the final compression matrix is  $\mathbf{T}_{\text{joint}} = \mathbf{U}^t$ . Modes with high singular values contain the bulk information about the

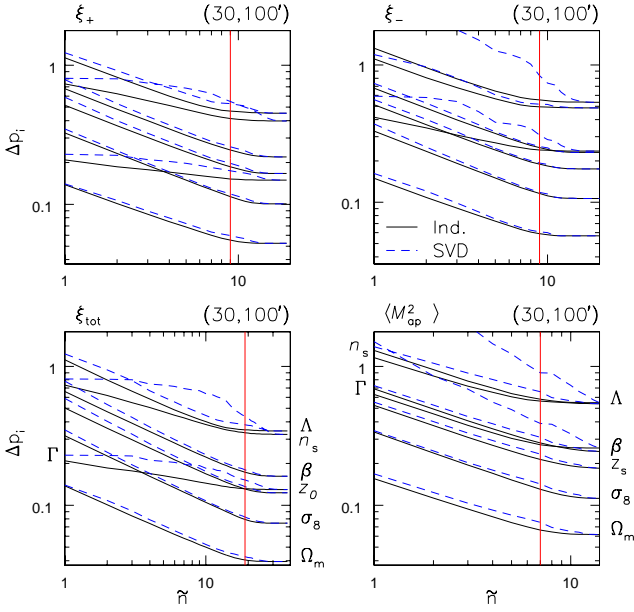


**Figure 2.**  $\Delta p_\alpha = (\tilde{F}_{\alpha\alpha})^{-1/2}$  as a function of the mode number  $\tilde{n}$  is plotted, according to (14) for the constant mean case and various cosmological parameters. Solid lines correspond to the independent parameter estimation (Sect. 2.4.1), dashed lines represent the joint parameter analysis (Sect. 2.4.4). The four panels correspond to the shear statistics  $\xi_+$ ,  $\xi_-$ , their combination  $\xi_{\text{tot}}$  and  $\langle M_{\text{ap}}^2 \rangle$  (see Sect. 3.1). The survey geometry is (30, 100'). The maximum mode number  $n$  equals the number of bins, which is 38 for  $\xi_{\text{tot}}$ , 19 for both  $\xi_+$  and  $\xi_-$  and 14 for  $\langle M_{\text{ap}}^2 \rangle$ .

cosmological parameters, whereas row vectors of  $\mathbf{T}_{\text{joint}}$  corresponding to vanishing or very small  $\sigma_i$  capture redundant or almost redundant information. Inserting  $\mathbf{T}_{\text{joint}}$  into (12), the Fisher matrix after the final compression is easily calculated.

If  $\tilde{n}_\alpha$  is the number of modes that were used in the optimisation process for the  $\alpha^{\text{th}}$  parameter, the joint matrix  $\mathbf{T}_{\text{joint}}$  has  $\tilde{n}' = \sum_{\alpha=1}^m \tilde{n}_\alpha$  columns. Based on the amplitude of the singular values, one can choose a final mode number  $\tilde{n}_{\text{joint}} < \tilde{n}'$  fixing the compression factor. As an example, the transformed diagonal elements of the Fisher matrix are plotted as a function of  $\tilde{n}_{\text{joint}}$  in Fig. 2, where the saturation plateau can be used to determine the final mode number.

Also for the constant covariance case (Sect 2.4.2), a joint parameter estimation analysis can be done. We combine the  $m$  eigenvectors resulting from the  $m$  individual parameter analyses to the  $n \times m$ -matrix  $\mathbf{T}$ , after having multiplied them by their respective eigenvalues. The singular value decomposition of  $\mathbf{T}$  will result in  $m$  singular values, which give us information of the degree of degeneracy between the parameters. We will discuss results for this analysis in Sect. 3.3.

#### 2.4.5 Window functions

The linear data compression defined in (11) generates a new data vector  $\tilde{\mathbf{x}}$  which in the case of single parameter optimisation represents a set of uncorrelated unit-variance Gaussian random variables (TTH). The components  $\tilde{x}_i$  of the new

data vector contain pairwise independent and uncorrelated information about cosmology. In our case the data consists of second-order shear statistics and the cosmological information is contained in the convergence power spectrum.

Using the KL eigenmode technique, we can study in detail how the power spectrum is sampled in order to yield uncorrelated data points. By comparing modes corresponding to high (low) eigenvalues, we can see which scales carry much (little) of the cosmological information.

For any second-order statistics, the dependence on the power spectrum is encoded in a window function. For the two shear 2PCF  $\xi_+$  and  $\xi_-$ , these are the broad-band Bessel functions  $J_0$  and  $J_4$ , respectively, see eq. (2); the filter function for the aperture mass statistics  $\langle M_{\text{ap}}^2 \rangle$  is the narrow-peaked function  $[24 J_4(\eta)/\eta^2]^2$ , see (3).

For each component  $\tilde{x}_i$  of the new data vector, we define a new window function  $W_i$ , which is a combination of the original filter functions associated to different smoothing scales  $\theta_j$ . In the case of the 2PCF, the new data vector is

$$\tilde{\xi}_i^\pm = T_{ij}^\pm \xi_\pm(\theta_j) = \frac{1}{2\pi} \int_0^\infty d\ell \ell P_\kappa(\ell) W_i^\pm(\ell);$$

$$W_i^\pm(\ell) = \sum_j T_{ij}^\pm J_{0,4}(\ell\theta_j). \quad (16)$$

Similarly, for  $\langle \tilde{M}_{\text{ap}}^2 \rangle$  we obtain the new window functions  $W_i^E(\ell) = \sum_j T_{ij}^E [24 J_4(\ell\theta_j)/(\ell\theta_j)^2]^2$ . In the case of the combined vector  $\tilde{\xi}^{\text{tot}} = (\tilde{\xi}^+, \tilde{\xi}^-)$ , the window functions  $W_i^{\text{tot}}$  are linear combinations of  $W_i^+$  and  $W_i^-$ .

In case of a constant mean, the rows of the matrix  $\mathbf{T}$  contain the  $\tilde{n}$  transposed eigenvectors  $\mathbf{b}$ , see Sect. 2.4.1. For the constant covariance case, there is only one eigenmode, in this case  $\mathbf{T}_0 = \boldsymbol{\mu}_{,\alpha}^t \mathbf{C}^{-t}$ . We denote all quantities corresponding to the constant covariance case with a subscript ‘0’, e.g.  $\tilde{\xi}_0^+$ ,  $W_0^+$  etc. For the joint parameter estimation (Sect. 2.4.4), window functions are defined analogously, by inserting the joint matrix  $\mathbf{T}_{\text{joint}}$  into eq. (16).

The study of these window functions, which is presented in the next section, will provide us with insights about how the convergence power spectrum is sampled in order to constrain cosmological parameters with cosmic shear. It allows us to investigate how different Fourier modes are probed by a given survey strategy.

## 3 NUMERICAL RESULTS

The impact of various survey strategies, noise structures and the effect of binning are considered in the determination of the eigenmodes. We study separately the constant mean case (see Sect. 2.4.1) and the constant covariance case (see Sect. 2.4.2). Eigenmodes associated with the independent analysis of a single parameter and the joint analysis of several parameters (see Sect. 2.4.4) are investigated.

### 3.1 The input data

Our input data vector  $\mathbf{x}$  is one of one the following second-order statistics of cosmic shear, as defined in Sect. 2.2:

1. The correlation function  $\xi_+(\theta_i)$  measured at various angular scales  $\theta_i$ . The covariance is denoted as  $\mathbf{C}_{++}$ .

2. The correlation function  $\xi_-(\theta_i)$  measured at various angular scales  $\theta_i$ . The covariance is denoted as  $\mathbf{C}_{--}$ .

3. The joint combination  $\xi_{\text{tot}}$  of both data vectors  $\xi_+$  and  $\xi_-$  where the joint covariance matrix  $\mathbf{C}_{\text{tot}}$  is constructed out of blocks  $\mathbf{C}_{++}$ ,  $\mathbf{C}_{--}$  on the diagonal and  $\mathbf{C}_{+-}$  and its transpose on the off-diagonal.

4. The aperture mass statistics  $\langle M_{\text{ap}}^2(\theta_i) \rangle$  for various aperture radii  $\theta_i$  and its covariance  $\mathbf{C}(M_+)$ .

These statistics are calculated from the convergence power spectrum using eqs. (2) and (3). For the 2PCF, we use 19 angular logarithmic bins, the smallest separation between two galaxies considered being 0.5 arcmin. Since the calculation of the covariances and their derivations are very time-consuming, we have chosen a rather small number of angular bins. The largest angular distance is determined by the survey geometry (Sect. 2.1) – for a patch geometry, we choose this to be slightly less than the patch diameter  $R$ . This is to avoid very large separations with small numbers of galaxy pairs, which caused our results to be unstable when we varied the binning.

The joint 2PCF data vector  $\xi_{\text{tot}}$  has 38 entries, corresponding to the two times 19 angular bins for  $\xi_+$  and  $\xi_-$ . We calculate the aperture mass  $\langle M_{\text{ap}}^2 \rangle$  for 14 different angular bins. The calculation of the covariance of  $\langle M_{\text{ap}}^2 \rangle$  as a weighted sum of the 2PCF covariances can be biased for small aperture radii, when for a given binning of the 2PCF only a small number of terms contribute to the sum. We take into account a smaller number of aperture radii than separations for the 2PCF.

## 3.2 Cosmological model and parameters

We include  $m = 7$  parameters in our analysis. These are  $\Omega_m$ , the power spectrum normalisation  $\sigma_8$ , the spectral index of the initial scalar fluctuations  $n_s$  and  $\Gamma$  which determines the shape of the power spectrum. In addition, the cosmological constant  $\Lambda$  is included in our analysis. The redshift distribution of source galaxies is assumed to be (Smail et al. 1995)

$$p(z)dz = \frac{\beta}{z_0\Gamma(3/\beta)} \left(\frac{z}{z_0}\right)^2 e^{-(z/z_0)^\beta} dz. \quad (17)$$

The parameters  $z_0$  and  $\beta$  are treated as free parameters to be determined from the data.

Our reference model is a flat  $\Lambda$ CDM Universe with  $\Omega_m = 0.3$ ,  $\Gamma = 0.21$ ,  $n_s = 1$  and  $\sigma_8 = 1$ . The source redshift distribution is given by  $z_0 = 1$  and  $\beta = 1.5$ , corresponding to a mean redshift of  $\sim 1.5$ . The CDM transfer function is taken from Bardeen et al. (1986), the non-linear power spectrum is calculated using the fitting formulae of Peacock & Dodds (1996).

## 3.3 KL eigenmode analysis

### 3.3.1 Error bars

For the case of a constant mean (Sect. 2.4.1), we plot the MVB  $\Delta p_\alpha = (\tilde{F}_{\alpha\alpha})^{-1/2} = (2/\sum_{k=1}^{\tilde{n}} \lambda_k^2)^{1/2}$  in Fig. 2 as a function of the compression mode number  $\tilde{n}$ , for both single and joint parameter estimation. Typically, the asymptotic limit is reached at a lower mode number in case of  $\tilde{\xi}^+$  compared to  $\tilde{\xi}^-$ . On the other hand, the joint use of  $\tilde{\xi}^+$  and  $\tilde{\xi}^-$

reduces the error bars by a factor of nearly two in most cases. The saturation limit is approximately the same for each of the individual cosmological parameters. Irrespective of the survey strategy, approximately the first half of eigenmodes contain virtually all information about each individual parameter, thus a compression factor of nearly two is possible without increasing the error.

The error bars attained by both the individual and the joint analysis of the 2PCF  $\xi_+$  and  $\xi_-$  are typically tighter compared to the  $\langle M_{\text{ap}}^2 \rangle$ -constraints for a given survey geometry.

We also conduct a joint parameter estimation for the case of a constant covariance (Sect. 2.4.2). The complete information of all seven cosmological parameters is encoded in the  $m = 7$  individual eigenmodes. However, the result of the SVD shows, that for  $\Omega_m, \sigma_8, z_0$  and  $\beta$  already the first singular mode carries basically all of the information on these parameters. For  $\Gamma, n_s$  and  $\Lambda$ , the saturation of the error is reached after two modes. Apparently, the first mode picks up most of the information about the first group of highly-degenerate parameters, the second one completes the information about the parameters from the second group. This picture is consistent with the correlation matrix of the parameters, as discussed in Sect. 3.3.3.

### 3.3.2 Window functions for the compressed eigenmodes

In Fig. 3 we plot the rank-ordered window functions  $W_i(\ell)$  associated with  $\Omega_m$  for the constant mean case. As an example, the first three window functions containing most of the information are compared with two higher order modes which contain less or negligible information. The survey strategy used in this analysis is a  $(30, 100')$ -patch geometry (see Sect. 2.1).

Because the window functions for  $\tilde{\xi}_i^+$  are linear combinations of  $J_0(\ell\theta_j)$ , there is always an extended tail which takes contributions from very large scales. The window functions for  $\langle M_{\text{ap}}^2 \rangle$  are very localized and each eigenmode samples only a small  $\ell$ -region. For all statistics, small scales are noise dominated and contribute with only small amplitude to higher-order, low signal-to-noise KL modes, see also Fig. 9.

The fact that the information content is larger for small  $\ell$  and decreases with  $\ell$  can be understood when considering the simple case in which the covariance matrices and its derivatives are diagonal. Then, the eigenproblem matrix  $\mathbf{A} = \mathbf{L}^t \mathbf{C}_\alpha \mathbf{L}^{-t}$  (13) is also diagonal with  $A_{kk} = (C_{,\alpha})_{kk}/C_{kk}$  being the eigenvalues. The diagonals of both  $\mathbf{C}$  and  $\mathbf{C}_\alpha$  are decreasing functions of the angular scale (except for small bumps due to geometrical survey effects). Since the decrease of  $\mathbf{C}_\alpha$  is in general shallower than  $\mathbf{C}$ , the largest eigenvalues occur on the largest angular scales.

For the constant covariance case (Fig. 6), the window functions  $W_0$  are much broader since there is only one eigenmode containing all information and taking contributions from all angular scales. The  $W_0$  peak at a median angular scale where the signal dominates over the noise both from the intrinsic ellipticity dispersion of galaxies at small angular scales and from the finite sky coverage at larger angular scales.

The strong degeneracy among various parameters is reflected in the behaviour of their associated window func-

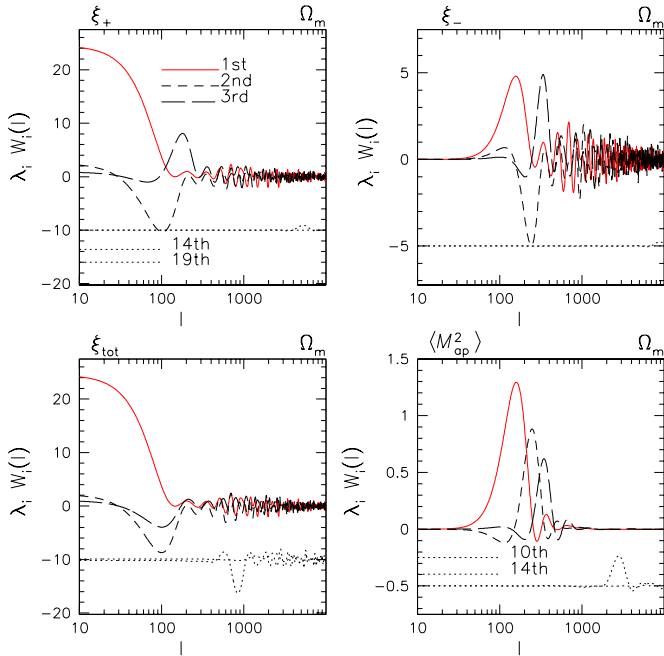


**Figure 3.** Window functions  $W_i(\ell)$  multiplied with the corresponding eigenvalues  $\lambda_i$ , associated with the individual determination of the parameter  $\Omega_m$ , for the constant mean case. The first three eigenmodes, representing the three highest signal-to-noise modes, and for comparison, two exemplary higher order eigenmodes ( $i = 14, 19$  for  $\xi_+, \xi_-$  and  $\xi_{\text{tot}}$ ;  $i = 10, 14$  for  $\langle M_{\text{ap}}^2 \rangle$ ) are plotted. The four panels correspond to the four different shear statistics as indicated. The specific survey strategy used in this case is a  $(30, 100')$  patch geometry (see Sect. 2.1). Note that the window functions for the two higher order modes have been displaced from zero to increase the visibility.

tions: for all four statistics, degenerate parameters have very similar curves (see next section for a discussion of the different near-degeneracies). The  $\Gamma$ - and  $n_s$ -filter functions have a zero-transition – the low  $\ell$ -plateau has opposite sign than the peak reflecting the sensitivity of these parameters to a tilt in the power spectrum.

Figure 6 displays for the dominant contribution to the Fisher matrix (second term in eq. 10) how individual Fourier modes are sampled and combined in an “optimal” way to constrain cosmological parameters as indicated. It shows on which scales the convergence power spectrum has the largest influence on the determination of cosmological parameters, depending on the survey strategy (see also Sect. 3.3.4). In a forthcoming paper, analogous analyses based on the present work will be performed for third-order statistics of cosmic shear, allowing one to quantify the sampling of the convergence bispectrum to extract cosmological information. Moreover, the scales of interest will be studied for a combined analysis of the power and the bispectrum which will reduce the near-degeneracies between parameters.

### 3.3.3 Correlation between cosmological parameters

In Fig. 7 we plot the correlation coefficient of the Fisher matrix  $r_{\alpha\beta} = \hat{F}_{\alpha\beta} / (\hat{F}_{\alpha\alpha} \hat{F}_{\beta\beta})^{1/2}$ , which quantifies the level of degeneracy between two parameters, as a function of the

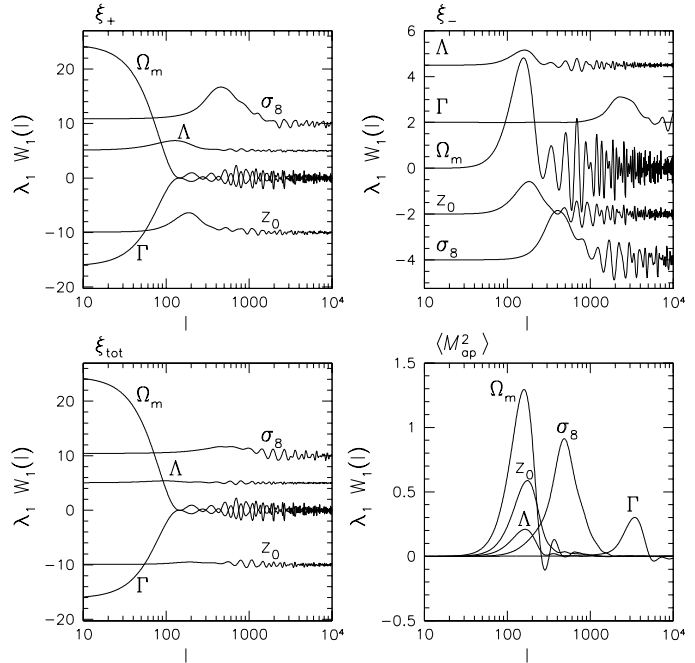


**Figure 4.** The dominant first window functions  $\lambda_1 W_1(\ell)$  for the constant mean case, associated with various parameters as indicated in the figure. The four panels correspond to the four different shear statistics as indicated. The survey strategy is  $(30, 100')$  (see Sect. 2.1). For visual clarity, some of the curves are shifted vertically.

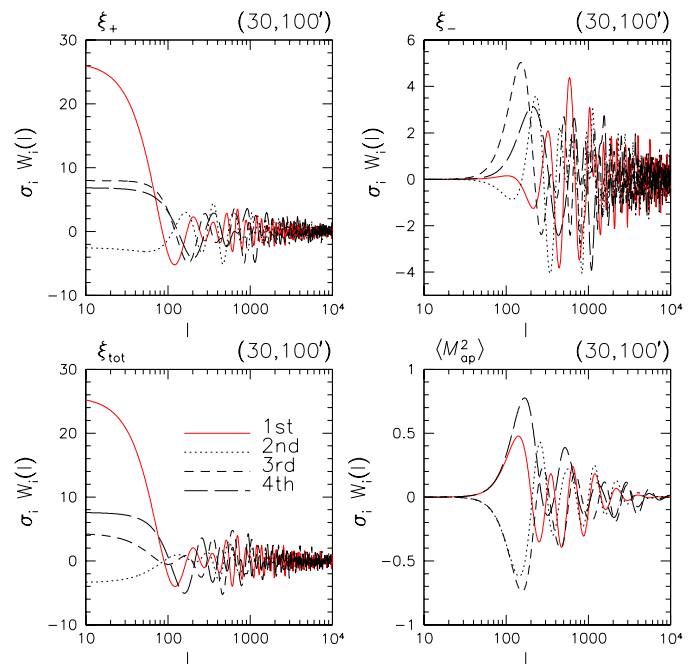


**Figure 5.** Window functions  $\sigma_i W_i$  for the joint analysis of all parameters using SVD in the case of constant mean. The first four singular modes multiplied by the corresponding singular values are displayed.



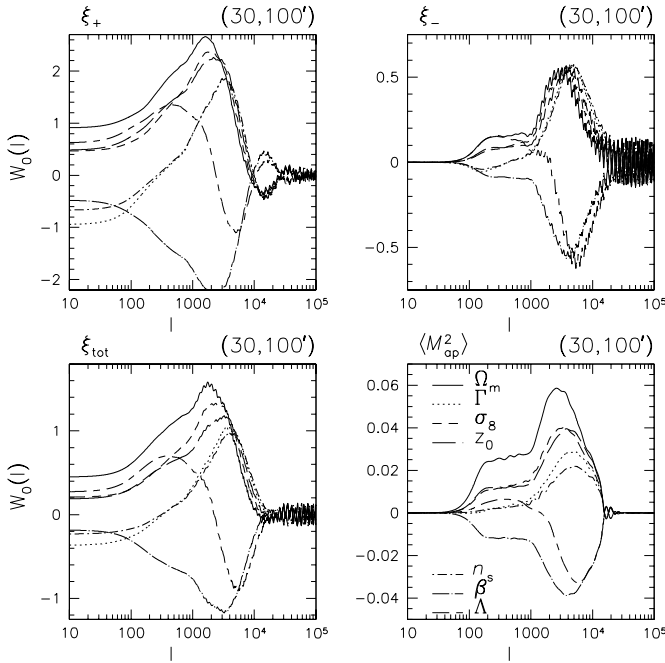


**Figure 6.** The window function  $W_0$  for the constant covariance case associated with various parameters as indicated in the figure. The four panels correspond to the four different shear statistics as indicated.

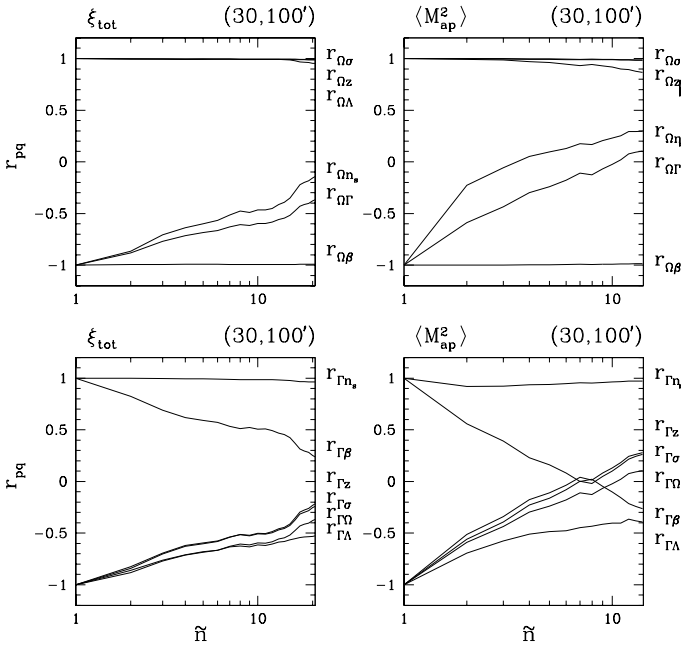


**Figure 7.** The correlation of  $\Omega_m$  (upper panels) and  $\Gamma$  (lower panels) with the other parameters, as a function of the mode number  $\tilde{n}'$  for the joint parameter estimation involving all parameters. The left and the right panels correspond to  $\xi_{\text{tot}}$  and  $\langle M_{\text{ap}}^2 \rangle$ , respectively.

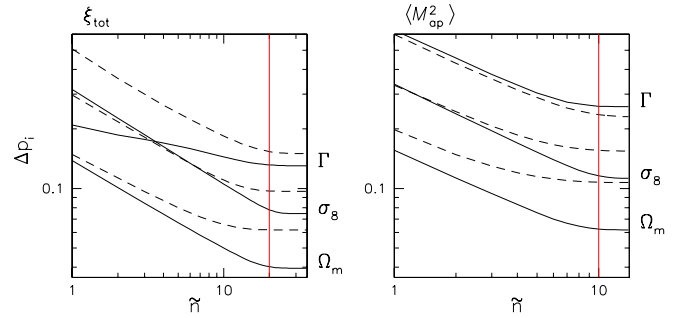


**Figure 8.**  $\Delta p_\alpha$  as function of the eigenmode number  $\tilde{n}$ , for the survey geometries  $(30, 100')$  (solid lines) and  $75 \cdot 26'^2$  (dashed lines). The single parameter case of  $\Omega_m$ ,  $\sigma_8$  and  $\Gamma$  is displayed.

compression mode number  $\tilde{n}$ . For very small mode numbers, the Fisher matrix becomes singular and all parameters are completely degenerate. Clearly, there exist two groups of highly-degenerate parameters ( $\Omega_m, \sigma_8, z_0, \beta, \Omega_\Lambda$ ) and ( $\Gamma, n_s$ ). For parameters from different groups, the correlation decreases, even for mode numbers  $\tilde{n}$  where the diagonal element has reached the plateau. Thus, redundant modes which do not carry any information regarding the Fisher diagonal are nevertheless important and help to reduce parameter degeneracies.

We also calculate the correlation coefficient  $r_{\alpha\beta}$  for the constant covariance case, where the SVD gives us only  $m = 7$  singular modes. The correlation coefficient forms a plateau when as few as two of the singular modes are included, as it is the case for the diagonal elements of the Fisher matrix (Sect. 3.3.1). However, even though  $\mathbf{F}$  does not change much when three modes and more are added, this is not true for the inverse Fisher matrix since  $\mathbf{F}$  is quite ill-conditioned and small changes have a large impact on  $\mathbf{F}^{-1}$ . For a numerically stable determination the MVBs from the inverse Fisher matrix, one needs as many modes as number of parameters.

### 3.3.4 Survey strategy

We plot  $\Delta p_\alpha$  as a function of the eigenmode number in Fig. 8. In contrast to Fig. 2, where we compared the single and the joint (SVD) parameter case for one survey strategy, we emphasize here on the single parameter estimation and compare the resulting errors for different survey geometries. All patch geometry strategies as well as the survey consisting of 12 uncorrelated  $65'^2$ -fields yield very similar results, the case  $(30, 100')$  is shown as a representative. On the contrary, the MVBs from the  $75 \cdot 26'^2$ -geometry are significantly higher with few exceptions. This latter survey does not sample medium and large scales in contrast to the patches and the  $12 \cdot 65'^2$  case. The small cosmic variance corresponding to the 75 independent lines of sight can not compensate for the lack of large-scale information.

The effect of survey strategy on the window functions is a shift in  $\ell$ , depending on the scales that are sampled by the survey (compare Fig. 5 with 10, and Fig. 6 with 11). For the constant mean case, the uncorrelated images-surveys shift the peaks of the  $\langle M_{\text{ap}}^2 \rangle$ -window functions corresponding to  $\Omega_m$  and the other parameters from this degeneracy group (Sect. 3.3.3) towards higher  $\ell$  whereas for  $\Gamma$  and  $n_s$ , the

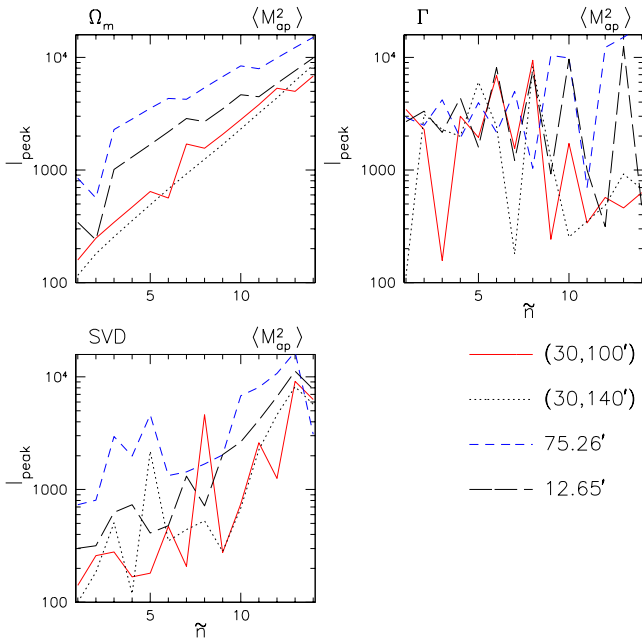


**Figure 9.** The peak position of the  $\tilde{n}^{\text{th}}$   $\langle \tilde{M}_{\text{ap}}^2 \rangle$ -windows as a function of the corresponding eigenmode number  $\tilde{n}$ , for single analysis of the parameters  $\Omega_m$  (upper left panel) and  $\Gamma$  (upper right), and for the joint estimation (lower panel).  $\theta_{\text{peak}} = 5/\ell_{\text{peak}} = 17'(1000/\ell_{\text{peak}})$  is the corresponding peak in real space.

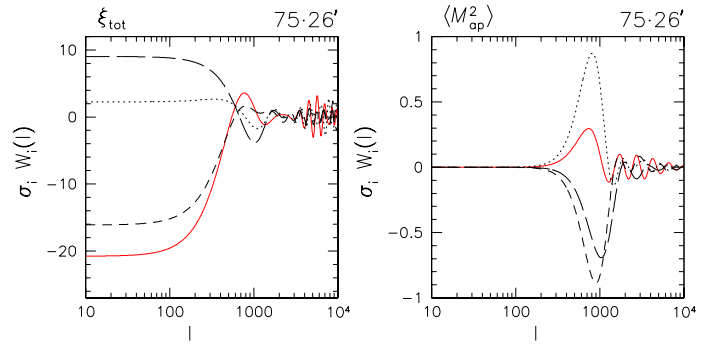
peaks seem to be randomly distributed, see Fig. 9. For the latter two parameters, there is no preference of large scales, apparently all scales contribute with the same importance to the Fisher matrix.

Figure 12 shows the window functions  $W_0$  for the joint parameter analysis, corresponding to the dominant constant covariance case. From this figure, it is clear that only the first two modes carry significant information about cosmology. The shapes of the two functions is complementary, for example, the second one has a zero transition at roughly the peak position of the first one. The reason is that there are basically two groups of parameters entering the convergence power spectrum, and the information content is described by two independent singular modes.

For various survey strategies, we calculate the simultaneous MVBs for  $\Omega_m, \sigma_8, \Gamma$  and  $n_s$  using (9). The patch geometries yield similar errors which are smaller than those from the uncorrelated images-surveys, see Table 3.3.4. In particular for  $\langle M_{\text{ap}}^2 \rangle$ , the lack of large scales of the  $75 \cdot 26'^2$  case results in a large uncertainty for  $\Omega_m$  and  $\sigma_8$ . This confirms a result found by Jain & Seljak (1997), stating that in order to break the  $\Omega_m$ - $\sigma_8$ -degeneracy, the shear correlation on large (linear) scales has to be added to the measurement of small (non-linear) scale correlation.

### 3.3.5 Noise levels

We determine the dependence of the Fisher matrix for different survey characteristics and noise levels. The calculations are done for a  $(30, 100')$ -patch survey geometry. We vary the survey area  $A$  between 1.4 and 14 square degrees, by adding more and more independent, uncorrelated patches, each con-



**Figure 10.** The first four window functions  $\sigma_i W_i$  for the joint parameter and constant mean case, corresponding to a  $75 \cdot 26'$  survey. See Fig. 5 for an explanation of the curves, and for comparison with a  $(30, 100')$  geometry.

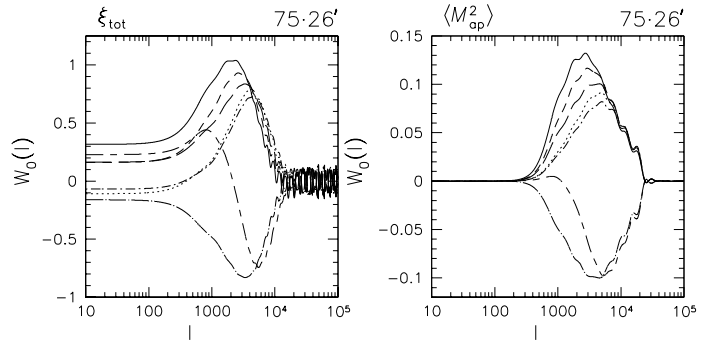


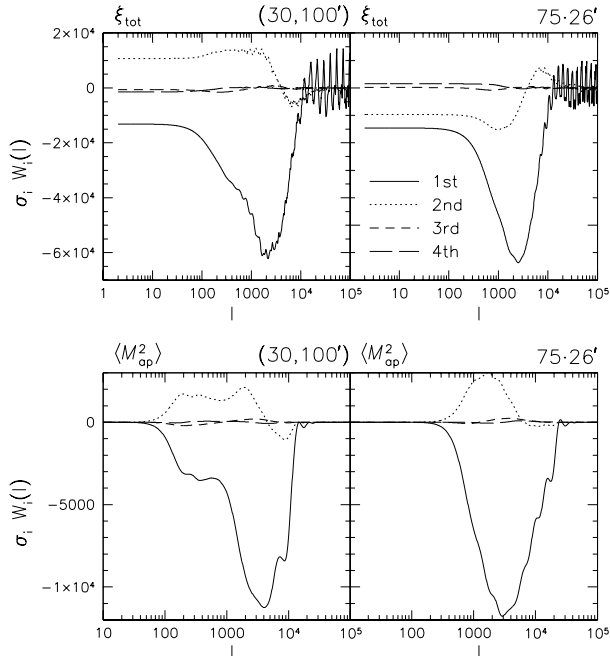
**Figure 11.** The constant covariance window functions  $W_0$  for the seven cosmological parameters, corresponding to a  $75 \cdot 26'$  survey. See Fig. 6 for an explanation of the different curves, and for comparison with a  $(30, 100')$  geometry.

**Table 1.** Simultaneous MVBs for various parameters and survey strategies.

	$\xi_{\text{tot}}$			
	$\Omega_m$	$\Gamma$	$\sigma_8$	$n_s$
$(60, 140')$	0.13	0.17	0.24	0.21
$(30, 140')$	0.14	0.17	0.26	0.21
$(60, 100')$	0.14	0.19	0.26	0.24
$(30, 100')$	0.14	0.18	0.26	0.22
$12 \cdot 65'^2$	0.17	0.22	0.30	0.27
$75 \cdot 26'^2$	0.18	0.23	0.33	0.26

	$\langle M_{\text{ap}}^2 \rangle$			
	$\Omega_m$	$\Gamma$	$\sigma_8$	$n_s$
$(60, 140')$	0.22	0.35	0.41	0.45
$(30, 140')$	0.27	0.40	0.49	0.50
$(60, 100')$	0.25	0.43	0.47	0.54
$(30, 100')$	0.28	0.46	0.53	0.57
$12 \cdot 65'^2$	0.28	0.47	0.53	0.56
$75 \cdot 26'^2$	0.37	0.53	0.69	0.58



**Figure 12.** The first four window functions multiplied by the singular values,  $\sigma_i W_i$ ,  $i = 1 \dots 4$ , for the joint analysis of constant covariance, corresponding to two survey strategies as indicated.

taining 30 images. For the variation of the other parameters (source ellipticity dispersion  $\sigma_\varepsilon$ , number of background galaxies  $n_{\text{gal}}$ , number of bins  $n$  and redshift parameter  $z_0$ ), a single patch was used to calculate the Fisher matrix. In the constant covariance case, we write the MVB as

$$\Delta p_\alpha = F_{\alpha\alpha}^{-1/2} = k \left( \frac{A}{10 \text{ sq deg}^2} \right)^{-0.5} \left( \frac{\sigma_\varepsilon}{0.3} \right)^\mu \times \left( \frac{n_{\text{gal}}}{30 \text{ arcmin}^{-2}} \right)^\nu \left( \frac{n}{20} \right)^\eta z_0^\lambda, \quad (18)$$

where the constant  $k$  and the power-law indices  $\mu, \nu, \eta$  and  $\lambda$  are given in Table 2 for each parameter  $\alpha$ .

Note that although the MVB for  $\langle M_{\text{ap}}^2 \rangle$  is smaller than the one for the 2PCF, this is not true when more than one parameter is considered. In that case, the MVB is given by the inverse of (a submatrix of) the Fisher matrix. The off-diagonal terms are typically larger for  $\langle M_{\text{ap}}^2 \rangle$  which decreases the diagonal of the inverse matrix.

If the mean is constant, the Fisher matrix is independent of the area of the survey. Except for the binning (see next section), the sensitivity of the other survey characteristics is weaker than for the constant covariance case. For our fiducial values of  $\sigma_\varepsilon = 0.3$ ,  $n_{\text{gal}} = 30 \text{ arcmin}^{-2}$ ,  $n = 20$  and  $z_0 = 1$ , the survey area where both terms in (10) are equal varies between 0.06 (for  $n_s$ ) and 0.4 ( $\Omega_m$ ) square degrees in the case of  $\xi_{\text{tot}}$ . For the aperture mass statistics, this area of equal contribution of both terms to the Fisher matrix is roughly a factor of 4 smaller. Thus, only for very small survey areas the constant mean term is important.

Noise at small angular scales is dominated by Poisson noise coming from the intrinsic ellipticity dispersion of the galaxies  $\sigma_\varepsilon$ , and the finite number density of galaxies  $n_{\text{gal}}$ . The effect of both error sources is shown in Fig. 13. The

**Table 2.** The coefficients describing the MVB for the constant covariance case as function of various survey characteristics, for different cosmological parameters, see (18).

$\xi_{\text{tot}}$					
Parameter	$k$	$\mu$	$\nu$	$\eta$	$\lambda$
$\Omega_m$	0.0074	-0.77	0.40	-0.03	0.52
$\Gamma$	0.0109	-1.28	0.71	-0.08	1.03
$\sigma_8$	0.0098	-0.96	0.52	-0.05	0.85
$z_0$	0.0157	-1.08	0.59	-0.06	-0.59
$n_s$	0.0237	-1.34	0.76	-0.09	1.04
$\beta$	0.0206	-1.09	0.59	-0.06	0.36
$\Lambda$	0.0498	-1.25	0.70	-0.09	0.50
$\langle M_{\text{ap}}^2 \rangle$					
Parameter	$k$	$\mu$	$\nu$	$\eta$	$\lambda$
$\Omega_m$	0.0073	-0.90	0.51	-0.02	0.70
$\Gamma$	0.0085	-1.20	0.67	-0.05	1.03
$\sigma_8$	0.0086	-1.03	0.58	-0.05	1.00
$z_0$	0.0131	-1.11	0.62	-0.04	-0.49
$n_s$	0.0184	-1.23	0.68	-0.04	1.00
$\beta$	0.0172	-1.11	0.62	-0.04	0.45
$\Lambda$	0.0424	-1.23	0.68	-0.06	0.24

information content of each eigenmode decreases with decreasing  $n_{\text{gal}}$  and increasing  $\sigma_\varepsilon$ . The asymptotic plateau is reached for marginal smaller mode numbers in the case of higher noise level. The resulting decrease in accuracy with which a given parameter is determined can be inferred from the asymptotic values.

### 3.3.6 Binning

We vary the number of angular bins  $n$  of the two-point correlation functions between 20 and 50, in order to quantify the effect on our results. For the constant mean case, the power-law decrease of the Fisher matrix diagonal are unaffected by the binning. We found the height of the plateau to weakly depend on the bin number, as  $n^{-\eta}$  where  $\eta$  is different for different statistics and parameters, and ranges between 0.18 and 0.3.

Note that the compression factor is somehow arbitrary since the number of bins can be chosen freely. However, within the (realistic) range that we tested, it is close to two. If we further increase the number of bins, the compression will of course increase; no new information will be added since the correlation between adjacent bins will approach unity for very small separations. The weak dependence of the plateau on  $n$  shows that we have not yet reached that saturation regime. If one considers the observed galaxy ellipticities as input data vector, the compression factor is of course much larger.

The Fisher matrix in case of constant covariance is only very weakly dependent on the bin number, as shown in the previous section (see Table 2). The diagonal elements of the Fisher matrix for both cases (constant mean/covariance) are shown in Fig. 14. In both the cases, for constant covariance and constant mean, the amplitude of the window functions increases with the number of bins. The shape is not affected by the binning.

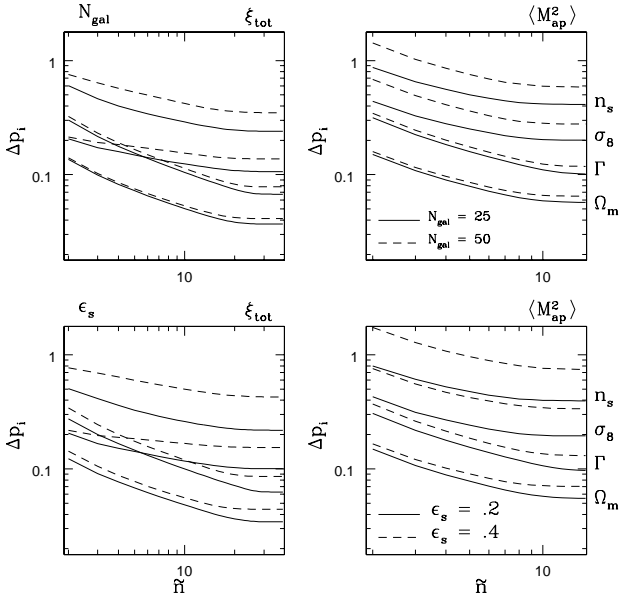


**Figure 13.**  $\Delta p_\alpha = (F_{\alpha\alpha})^{-1/2}$  as a function of the number of modes  $\tilde{n}$  as in (14), for different noise levels. *Upper panels:*  $n_{\text{gal}} = 25 \text{ arcmin}^{-2}$  (solid lines),  $n_{\text{gal}} = 50 \text{ arcmin}^{-2}$  (dashed lines). *Lower panels:*  $\sigma_\epsilon = 0.2$  (solid lines),  $\sigma_\epsilon = 0.4$  (dashed lines). The left panels corresponds to the joint correlation function  $\xi_{\text{tot}}$  whereas in the right panels results for  $\langle M_{\text{ap}}^2 \rangle$  are shown. The plots are done for the parameters  $\Omega_m, \sigma_8, \Gamma$  and  $n_s$ . The survey geometry is a single  $(30, 100')$  patch.

#### 4 DISCUSSION

We study the Karhunen-Loève generalised eigenmode problem in the context of weak lensing surveys. Four combinations of second-order shear statistics estimated at various angular scales are used as input data vectors – these are the 2PCFs  $\xi_\pm$ , their combination  $\xi_{\text{tot}}$  and the aperture mass dispersion  $\langle M_{\text{ap}}^2 \rangle$ . Different realistic survey geometries are considered to study the impact of noise and finite sky coverage for these estimators. We examine the dependence of both the mean and the covariance of these estimators on various cosmological parameters and the source galaxy redshift distributions. A Fisher matrix analysis is presented to determine errors associated with the estimation of various cosmological parameters and their cross-correlation with survey parameters.

We consider two different scenarios. In one case, the mean of second-order shear estimators is used to constrain the cosmological parameters while the covariance is constant and independent of cosmology. The second case uses the covariance of these estimators to constrain cosmological parameters assuming a constant mean. We study the information content of KL eigenmodes in both cases for various parameters. For the constant mean case, there are several eigenmodes among which the information is distributed; however, there is only one eigenmode associated with the constant covariance case which contains the complete information. The resulting error bars are anti-proportional to the square root of the survey area for the constant covariance case, and independent of the survey area if the mean is constant. Thus, for reasonable sky coverage (more than

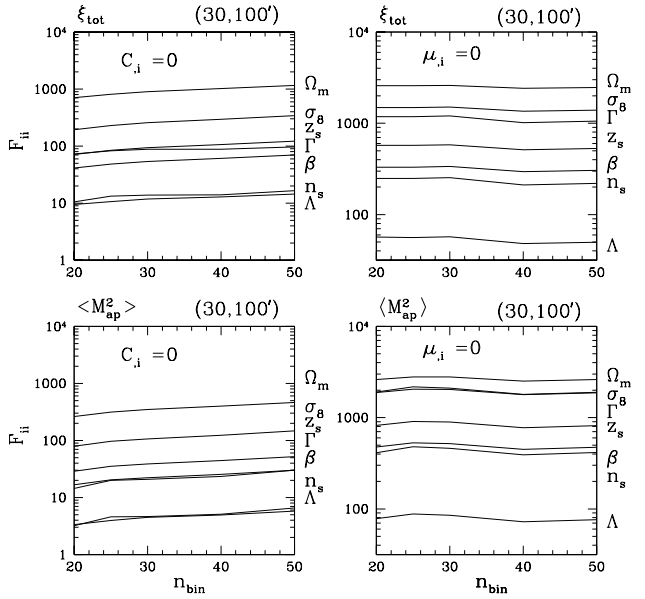


**Figure 14.** Effect of the bin number  $n$  on the Fisher matrix in the constant mean case for various estimators as indicated in the panels.

about 0.4 square degrees) the first case dominates over the second and the bulk part of the cosmological information is collected in only one mode.

From the results of our KL eigenmode analysis we find that, starting from  $n$  binned values of second-order shear statistics, a compression factor of almost two can be achieved in most cases without information loss, if the cosmological parameters are determined using the covariance. KL analysis provides rank-ordered, uncorrelated eigenmodes and corresponding window functions in the case of single parameter estimation. These sets of window functions provide cleanest measures of the projected power spectrum for a specific survey strategy. The first eigenmodes contain most of the information that one can extract and directly use for maximum-likelihood studies to constrain cosmological parameters. Typically, the error bars on individual parameters using the covariance are smallest when the joint correlation function  $\xi_{\text{tot}}$  is used.  $\xi_+$  gives better constraints than  $\xi_-$  which is in turn better than the aperture mass statistics  $\langle M_{\text{ap}}^2 \rangle$ .

We provide both an independent study of different parameters as well as a joint analysis of all parameters for each of these two cases (constant mean and constant covariance). The parameters which are near-degenerate have similar KL eigenfunctions. Among the five cosmological parameters we have considered,  $(\Omega_m, \sigma_8)$  and  $(\Gamma, n_s)$  show similar levels of degeneracy and have very similar eigenmodes. Moreover, the parameters characterising the source galaxy redshift distribution ( $z_0$  and  $\beta$ , see (17)) are degenerate to a high level with  $\Omega_m$  and  $\sigma_8$ .

It may be useful to note that additional constraints may be put by including higher-order statistics which will be left for further studies. Moreover, since the number of observables increases with increasing order (i.e. the shear three-point correlation function has eight independent components and depend on triangle configurations, Schneider &

Lombardi 2003), data compression can be useful and even necessary.

The eigenmodes associated with  $\Omega_m$  and  $\sigma_8$  mainly focus on larger angular scales where cosmological information is not contaminated by noise on small scales. On the other hand,  $\Gamma$  and  $n_s$  measure the shape of the projected matter power spectrum which is easier to determine when also information on smaller angular scales is available. Therefore the eigenmode windows associated with these two parameters tend to take more contributions from smaller scales. In contrast, the eigenmodes associated with the constant covariance case take contributions from virtually all angular scales probed by the survey and reaches a maxima roughly at medium angular scales where the signal dominates over both shot noise and scatter due to finite sky coverage.

Higher order KL modes do not carry any useful information and approximately half of the modes contain all of the information content of the Fisher matrix for a constant mean. However, the off-diagonal terms of the Fisher matrix which encode the cross-correlation among various parameters are also a function of the number of modes we include to reconstruct the Fisher matrix. We found that these terms keep evolving even after the diagonal terms have already reached a saturation limit. For very small numbers of modes the reconstructed Fisher matrix becomes singular, since the information sampled in only the few eigenmodes is too little in order to put constraints on more than one parameter, thus different cosmological parameters become completely degenerate.

The joint analysis of all seven parameters being estimated from the mean only (constant covariance) shows that only two eigenmodes (out of seven) are needed to constrain the parameters and to lift their near-degeneracies as far as possible.

In our analysis involving KL eigenmodes we have not included and modelled any systematic measurement errors. We have assumed that the errors are dominated by Poisson noise and intrinsic ellipticity noise at small scales and cosmic variance at larger angular scales. The covariance of the second-order shear statistics include all these noise sources, which are exact if the shear is a Gaussian field. Non-Gaussianity leads to an under-estimation of the noise on angular scales between 1 and 10 arc minutes.

Although the exact implementation of the survey geometry makes our approach more realistic, we still ignore B-mode contamination due to systematic residuals. This is mainly due to the absence of a specific model for the B-mode power spectrum in the case of systematic measurement errors. Such issues will have to be included in future studies. Although effects like intrinsic galaxy alignment and source clustering, which also cause a B-mode, can be and have been modelled (Crittenden et al. 2001; Croft & Metzler 2001; Heymans et al. 2004; Schneider et al. 2002), their contribution to the shear signal is secondary.

Incorporation of (photometric) redshift information will in general improve the accuracy with which cosmological parameters can be recovered. However, we have not divided the source galaxies into redshift bins, because of the corresponding complication in the calculation of the covariance. However, this is possible in principle, e.g. using correlated Gaussian fields, see e.g. Simon, King & Schneider 2004. The inclusion of non-Gaussian terms in the Fisher matrix anal-

ysis (Taylor & Watts 2001) will invariably help us to break some of the parameter degeneracies which we have studied here. However, the construction of covariance matrices associated with various third-order estimators tend to be very cumbersome. Although certain analytical calculations were made recently under simple assumptions (Munshi & Coles 2003; Munshi & Valageas 2005), more detailed analyses which incorporate realistic survey geometries remain to be done.

We incorporated the non-linear model of the power spectrum according to Peacock & Dodds 1996. In a forthcoming work, an improved version based on the halo model, e.g. halofit (Smith et al. 2003) will be used. In addition, baryonic physics, non-zero neutrino masses and a varying dark energy equation-of-state parameter will be taken into account.

A simple-minded signal-to-noise eigenmode analysis (an interesting special case of KL eigenmode analysis, see TTH) is difficult to perform for the case of the covariance matrices we have considered. This is because of the difficulty in separating the signal and noise contributions in the covariance matrices. Where as the  $\mathbf{V}$  terms (cosmic variance) are pure signal and the  $\mathbf{D}$  terms (shot noise) is pure noise, it is difficult to separate the mixed terms  $\mathbf{M}$  with such clarity. Increasing the noise contribution either by increasing the intrinsic ellipticity dispersion of galaxies  $\sigma_e$  or by decreasing the number density of source galaxies  $n_{\text{gal}}$  results in a decrease in the information content of each of the KL eigenmodes. In addition the number of eigenmodes which contain useful information reduces, too.

## ACKNOWLEDGMENTS

MK was supported by the Deutsche Forschungsgesellschaft (DFG) under the project SCHN 342/3-1. MK thanks Peter Schneider and Peter Watts for helpful discussions and useful comments on the manuscript. DM was supported by PPARC of grant RG28936. It is a pleasure for DM to acknowledge many fruitful discussions with members of Cambridge Leverhulme Quantitative Cosmology Group as well as member of Cambridge Planck Analysis Center. DM also benefitted from useful discussion with Patrick Valageas, Alan Heavens and Lindsay King. We wish to thank the anonymous referee for useful suggestions and comments which led to a substantial improvement of the paper.

## REFERENCES

- Bacon D., Réfrégier A., Ellis R.S., 2000, MNRAS, 318, 625
- Bartelmann M., Schneider P., 2001, Phys. Rep., 340, 291
- Bardeen J.M., Bond J.R., Kaiser N., Szalay A.S., 1986, ApJ, 304, 15
- Bond J.R., 1995, Phys. Rev. Lett., 74, 4369
- Bunn E.F., 1995, PhD thesis, U.C. Berkeley
- Contaldi C.R., Hoekstra H., Lewis A., 2003, Phys. Rev. Lett., 90, 221303
- Croft R.A.C, Metzler C.A., 2001, ApJ, 546, 561
- Crittenden R., Natarajan P., Pen U.-L., Theuns T., 2001, ApJ, 559, 552
- Hamilton A.J.S., Tegmark M., Padmanabhan N., 2000, MNRAS, 317, L23
- Heavens A., 2003, MNRAS, 343, 1327

- Heymans C., Brown M., Heavens A., Meisenheimer K., Taylor A., Wolf C., 2004, MNRAS, 347, 895
- Hoffmann Y., Zaroubi S., 2000, ApJ, 535, L5
- Hu W., 1999, ApJ, 522, L21
- Hu W., Tegmark M., 1999, ApJL, 514, L65
- Huterer D., White M., 2005, submitted to PRD, also astro-ph/0501451
- Ishak M., Hirata C., McDonald P., Seljak U., 2004, PRD, 69
- Jain B., Seljak, U., 1997, ApJ, 484, 560
- Kaiser N., 1992, ApJ, 388, 272
- Kaiser N., 1995, ApJ, 439, L1
- Kaiser N., Wilson G., Luppino G., 2000, ApJ, 537, 555
- Karhunen K., 1947, Ann. Acad. Sci. Fennicae Ser. A. I. 37
- Kendall M.G., Stuart A., 1969, The Advanced Theory of Statistics, Vol. II (London:Griffin)
- Kilbinger M., Schneider P., 2004, A&A, 413, 465
- Loève M., 1948, Processes Stochastiques et Mouvement Brownien, (Hermann, Paris France)
- Maoli R., van Waerbeke L., Mellier Y., Schneider P., Jain B., Bernardeau F., Erben T., Fort B., 2001, A&A, 368, 766
- Mastsubara T., Szalay A.S., Landy S.D., 2000 ApJ, 535, L1
- Mellier Y., 1999, ARA&A, 37, 127
- Munshi D., Coles P., 2003, MNRAS, 338, 846
- Munshi D., Valageas P., 2005, MNRAS, 356, 439
- Peacock J.A., Dodds S.J., 1996, MNRAS, 280, L19
- Réfrégier A., Rhodes J., Growth E.J., 2002, ApJ, 572, L131
- Réfrégier, A. 2003, ARA&A, 41, 645
- Schneider P. 1996, MNRAS, 283, 837
- Schneider P., Lombardi, M., 2003, A&A, 397, 809
- Schneider P., van Waerbeke L., Jain B., Kruse G. 1998, MNRAS, 296, 873
- Schneider P., van Waerbeke L., Kilbinger M., Mellier Y., 2002, A&A, 396, 1
- Schneider P., van Waerbeke L., Mellier Y., 2002, 398, 729
- Seljak, U., 1998, ApJ, 506, 64
- Simon P., King L.J., Schneider P., 2004, A&A, 417, 873
- Soccimarro R., Zaldarriaga M., Hui L. 1999, ApJ, 527, 1
- Silberman L., Dekel A., Eldar A., Zehavi, I., 2001, ApJ, 557, 102
- Smail I., Hogg D.W., Yan L., Cohen, J.G., 1995, ApJ, 449, L105
- Szalay A.S. et al., 2003, ApJ, 591, 1
- Taylor A., Watts P., 2001, MNRAS, 328, 1027
- Tegmark M., Taylor A., Heavens A., 1997, ApJ., 480, 22 (TTH)
- Tereno I., Doré O., van Waerbeke L., Mellier Y., 2005, A&A, 429, 383
- van Waerbeke L. et al., 2000, 358, 30
- van Waerbeke L., Mellier Y., 2003, in Valls-Gabaud D., Kneib J.P., eds., ASP Conf. Ser., Gravitational lensing: A unique tool for cosmology
- van Waerbeke L., Mellier Y., Hoekstra H., 2005, A&A, 429, 75
- van Waerbeke L., Mellier Y., Pelló R., Pen U.-L., McCracken H.J., Jain B., 2002, 393, 369
- Wittman D.M., Tyson J.A., Kirkman D., Dell'Antonio I., Bernstein G., 2000, Nature, 405, 143
- Vogele M.S., Szalay A.S., 1996, ApJ, 465, 34
- Watkins R., Feldman H.A., Chambers S.W., Gorman, P, Melott, A.L., 2002, ApJ, 564, 534